This is an preprint of an article published in AIChE Journal 56(1) 2-10 (2010), DOI: http://dx.doi.org/10.1002/aic.11969.

Terminal and Transient Drop Rise Velocity of Single Toluene Droplets in Water

Mirco Wegener and Matthias Kraume

Chair of Chemical Engineering, Technische Universität Berlin, Ackerstraße 71-76, D-13355 Berlin, Germany

Anja R. Paschedag

University of Applied Science Berlin, Luxemburger Str. 10, D-13353 Berlin, Germany

The knowledge of the drop rise velocity in dispersed systems is of fundamental importance. Especially the residence time is needed for calculation of mass transfer rates in extraction columns. The present work deals with fluid dynamic measurements of toluene droplets rising in water ranging from 1.0 to 7.0 mm, with the premise of high purity of the used chemicals. The toluene/water-system is widely used as a test system with high interfacial tension. A semi-empirical correlation for pure systems to predict the terminal velocity of single rising/falling droplets based on experimental data is presented. Results show that a distinction between maximum and characteristic mean values of the drop rise velocity is necessary, especially in the diameter range 2.4 - 3.0 mm where unexpected velocity fluctuations occur. Two distinct terminal rise velocities were observed for 3 mm droplets. Furthermore, comparisons of the Weber-Reynolds-correlation and the drag coefficient with correlations from literature show good agreement.

Keywords: terminal drop rise velocity, drag coefficient, oscillation, deformation, liquid-liquid extraction

Introduction

The rate of rise or fall of droplets in another immiscible liquid is of central importance in a variety of liquid-liquid extraction processes. In these contactors, one phase is dispersed into a second one, the mass transfer coefficient and the stage efficiency are closely related to drop size and drop rise velocity. Although droplet swarms rather than single droplets occur in such contactors, the understanding of fluid dynamic behaviour of single fluid particles is the basis for further investigations. Hence, the terminal velocity and the drag coefficient respectively are of fundamental importance to characterize the fluid dynamics of a given system.

The fluid dynamics of droplets or bubbles moving in other continuous media is of very complex nature. In contrary to rigid particles, fluid particles have a mobile interface, and the tangential shear stress exerted by the continuous fluid on the interface leads to internal circulation patterns, provided these interfacial movement is not hindered by contaminations. The capability of interfacial movements reduces the drag and increases the particle velocity compared to a rigid sphere.[1] As a consequence of the formation of an internal circulation, the mass transfer rate is significantly increased.[2-4] Impurities or surfactants of sufficient concentration can form a stagnant cap or completely hinder interfacial motion which increases the drag coefficient and thus decrease the terminal velocity,[5-8] in extreme case to the terminal velocity of a rigid sphere.

Solutal or thermal Marangoni effects can also have a strong influence on the interfacial motion. Additional shear stresses reduces the relative velocity between the two phases and are able to disturb the internal circulation.[7,9] The presence of Marangoni effects couples mass and momentum transfer in a complex manner since mass or heat transfer now affects the flow field and vice versa.

If the Weber number is high enough, shape deformation may occur according to the local stresses on the particle surface.[10] Shape deformation affects the drag coefficient (and thus the terminal velocity) on the one hand and the interfacial area (and thus the mass transfer rate) on the other hand. It has to be pointed out that droplets or bubbles in carefully purified systems are more deformed than in normal systems.[11]

Analytical solutions are only available for simple cases, therefore correlations based on experiments are necessary to predict terminal velocities or drag coefficients. The fluid dynamics of liquid drops moving in another liquid has been investigated by a variety of research groups. Numerous correlations for terminal velocities and drag coefficients were proposed,[12-14] the most famous is surely the generalized correlation of Reynolds number versus Eötvös number.[11] More useful for practical applications would be an explicit

formulation of the terminal velocity as a function of drop diameter, $v_t = f(d_P)$, since in Reynolds number correlations, the terminal velocity is needed which is a priori unknown.

One of the main problems is the fact that experimental results of the same system can vary dramatically from one research group to the next. This is mainly attributed to the above mentioned impurities, and in most cases, the degree of contamination is not known or communicated, which makes comparisons difficult. Therefore, most of the well-known correlations are based on unpurified systems. For convenience, correlations for pure systems are approached by modifying those obtained from contaminated systems.

The objective of the present paper is to derive a correlation for the rise velocity of toluene droplets in water from experiments where major effort has been made to prevent the system from contaminations. The semi-empirical approach presented by Grace et al.[11], see Eq. (A-5) in the Appendix, is adopted where the correlation for the terminal velocity in contaminated systems is modified with a correction function. A number of sequences is recorded for each drop diameter using a high-speed camera system. Therewith, the instantaneous velocity and velocity fluctuations can be captured. The investigated parameter range is 1.0 mm $\leq d_P \leq$ 7.0 mm or in dimensionless numbers: $0.038 \leq Eo \leq 1.85$ and $0.046 \leq We \leq 4.86$. Based on the terminal drop rise velocity, the drag coefficient can be calculated and compared with correlations proposed in literature (see Eqs. (A-6) to (A-10) in the Appendix). Finally, the Weber-Reynolds correlation,[15] see Eq. (12), developed for bubbles in aqueous media is tested and finally applied for the toluene/water system.

Experimental

The experimental setup shown in Fig. 1 is the same as described in Wegener et al..[16] The height and diameter of the glass column (1) are 1000 mm and 75 mm, respectively. The column is equipped with a jacket (2) which is filled with glycerol (with a refraction index similar to borosilicate glass) to allow for ideal optical access. The temperature of the system is adjusted with a RK 20 thermostat by LAUDA® (3) to 25°C. A Hamilton® PSD/2 module (4) is used to generate drops of a specified volume at a nozzle (5). Drop release is then accomplished automatically by a solenoid device (6). Therewith it was possible to generate any desired droplet diameter.

Position of Fig. 1

Three different types of nozzles have been used (see Table 1), a self-made glass nozzle for small droplets, a glass nozzle provided by Hilgenberg® with an inner diameter of 0.5 mm for intermediate droplet size, and a steel nozzle has been used for droplet diameters ≥4.8 mm.

Position of Table 1

Before each run, the organic and the aqueous phase are mutually saturated in a stirred tank (7) in order to avoid mass transfer between toluene and water during the experiment. The system is highly sensitive to impurities and quality of the chemicals, thus only chemicals of high purity have been used (toluene p.a. ≥ 99.9 %, deionized water with a specific resistance of 18.3 MΩ·cm). Physical properties[17] are listed in Table 2. In addition, only the materials PTFE, glass and stainless steel were used. To guarantee the purity of the system, a precise cleaning procedure has been accomplished. The column and all other relevant parts (saturation tank, column, tubes, syringes etc.) were cleaned mechanically and rinsed intensely before use. To check the system purity, 2 mm test droplets are used and compared to numerical simulations.[18] If the agreement is satisfactory, one set of experiments is conducted.

Position of Table 2

The instantaneous drop rise velocity was obtained from a high-speed camera device. A Photonfocus® MV-752-160 high-speed camera (8) with a ⅔"-CMOS sensor has been used, a second one is placed perpendicular to the first one. A spatial resolution of 752x70 pixels and a frame rate of f = 100 Hz was used in all investigations. The camera positions are perpendicular to the column, and the entire particle path through the column can be captured. The illumination system (9) consists of two simple fluorescent lamps (P = 30W each) with low thermal radiation for each camera. Two power supply units by Tridonic® operating at 40 kHz provide a constant brightness. The image processing tool Image-Pro Plus® 5.1 by Media Cybernetics has been used for image analysis. The recorded sequence is stored via the framegrabber on the hard disc of a computer (10). A reference frame is subtracted from each original image of the sequence and transformed into a binary image using a threshold procedure. The result is a table with the vertical and horizontal position of the mass centre of the drop for each frame. With these information, the drop rise velocity can then be calculated.

This is an preprint of an article published in AIChE Journal 56(1) 2-10 (2010), DOI: http://dx.doi.org/10.1002/aic.11969.

In the next section, the labels maximum velocity v_{max} and characteristic mean velocity v_{cha} will be used. They are defined as follows (see Fig. 2): the maximum drop rise velocity is the mean velocity of all maximum velocities of the recorded sequences for one droplet diameter (at least 15 sequences). The maximum velocity preferably occurs after the first acceleration after drop release from the nozzle. For some droplet diameters, the velocity started to oscillate around a lower value v_{cha} after the maximum velocity was attained. The characteristic mean velocity is calculated by the time Δt needed to pass the travel distance h_{tr}:

$$v_{cha} = \frac{h_{tr}}{\Delta t} \tag{1}$$

The travel distance begins where the maximum oscillation is over and ends when the upper end of the column was reached. All characteristic mean velocities of all recorded sequences of one diameter are then averaged.

Position of Fig. 2

The rise velocities of 35 different drop diameters ranging from 1.0 to 7.0 mm have been measured. With nozzle N_1, droplets from 1.0 to 3.6 mm were accomplished (17 diameters in total), with nozzle N_2 droplet diameters ranges from 2.0 to 5.0 mm (19 diameters in total, overlapping partly with N_1 and N_3), and nozzle N_3 led to droplets between 4.8 and 7.0 mm (12 diameters in total, overlapping partly with N_2). All experiments were repeated at least 15 times in order to satisfy statistical significance. In addition, some experiments were repeated on three different days with fresh dispersed and continuous phase. For all measurements, the reproducibility was found to be excellent.

Results and discussion

Transient and terminal drop rise velocity

Fig. 3 shows six diagrams of the transient drop rise velocity for different droplet diameters. In Fig. 3a and 3b, only one sequence out of 15 is shown for each diameter for convenience. In Fig. 3c, 15 sequences are shown for nozzle type N_1, Fig. 3d contains 15 sequences for nozzle type N_2. Fig. 4 summarizes the terminal velocities (maximum and characteristic mean values) obtained from the transient measurements

for the three nozzles. Additionally, the terminal velocity calculated from the correlation proposed by Grace et al.,[11] Eq. (A.1), is shown for comparison. This correlation has been derived from a variety of different liquid-liquid systems where contaminations had not been sufficiently avoided. From the figure it is obvious that higher velocities are obtained with the present system and contamination effects are substantially less pronounced.

For small droplets (d_P < 2.2 mm), see Fig. 3a, no significant shape deformation occurs, consequently the droplets accelerate after release from the nozzle tip to their terminal velocity. The velocity remains constant, no contaminations accumulate at the interface indicating a clean system. For d_P = 2.2 mm, velocity oscillation occurs shortly after drop release. But Weber numbers are too low, surface forces are stronger than inertia forces. In this case, the drop is elongated at the nozzle tip only due to drop release. Consequently, the shape changes from prolate to oblate spheroid, but the deformation is quickly dampened. The velocity becomes constant after 4 seconds and no further oscillations occur.

The situation is suddenly different in Fig. 3b (d_P = 2.4, 2.6 and 2.8 mm, nozzle N_2. The results are more or less the same for nozzle N_1.). After drop release, the velocity attains a distinct maximum. Then, the velocity decreases rapidly and oscillates around a lower value. In contrary to 2.2 mm droplets, the velocity remains at this lower level. Consequently, the characteristic mean velocity is significantly lower than the maximum velocity (see Fig. 4). Note that these experiments and those for d_P = 3.0 mm have been repeated three times on different days with fresh dispersed and continuous phase. The results were confirmed in all experiments. This result is in some way unexpected, since Weber numbers are still too small (We < 2) for significant shape deformation. When the diameter is increased to 3.0 mm, the situation becomes even more interesting, see Fig. 3c. If nozzle N_1 is used, the oscillation disappears although Weber and Eötvös number are higher than for smaller droplets. Visual observation shows that 3.0 mm droplets are oblate and thus deformed, but drop shape is preserved. Consequently, the maximum and characteristic mean velocity are close to each other, and, if characteristic mean velocities are considered, a sudden increase in terminal velocity can be stated (see Fig. 4) when compared to d_P = 2.8 mm.

Position of Fig. 3

Things are getting more complicated for nozzle N_2 (see Fig. 3d). Here, the velocity can achieve two distinct values. Either the velocities do not oscillate in accordance with the results for nozzle N_1, or they do oscillate around a lower value. Obviously, the drop is able to move in two different hydrodynamic

regimes. A comparable bifurcation (and thus a sudden increase in terminal velocity) was observed by Thorsen et al.[19] for methylene bromide drops (and for two other organics as well) falling in water. The authors excluded shape oscillation as an explanation for this result since faster droplets oscillated and the slower ones did not. Oscillations are expected to increase the drag coefficient which was not the case in their experiments. Thorsen et al. argue that the sudden increase was due to a transition from a state of non-circulation to a state of internal circulation. But this explanation seems to be doubtful since even smaller droplets do have an internal circulation.

Wu & Gharib[20] and also Tomiyama et al.[21] observed multiple terminal conditions for bubbles rising in water depending on the initial shape deformation. A large nozzle caused small initial shape deformation, a small nozzle large initial shape deformation. For a nozzle with small initial shape deformation the terminal velocity was lower than for those bubbles released at a nozzle with large initial shape deformation. Tomiyama et al.[21] attribute this effect to a certain nonlinearity in the Navier-Stokes equation due to a mutual coupling of fluid dynamic effects caused by the bubble interface on one hand and effects on the flow field by the motion of the bubble itself on the other hand. The authors speculate that the effect might be associated with the surface free energy σA and propose further studies on this issue. Yang et al.[22] investigated the effect of initial shape deformation of 1.2 mm air bubbles rising in water in a numerical study. This diameter showed different terminal velocities as reported by Wu & Gharib.[20] No difference was found in the terminal velocity and the reason remains unclear.

An answer to this bifurcation phenomena cannot be given here as well, but one aspect should be noted: In our experiments, the smaller nozzle N_1 produces drops with small initial shape deformation while nozzle N_2 generates a higher initial shape deformation. This is due to the larger contact area between the formed droplet and the dispersed phase remaining inside the nozzle, thus adhesive forces are higher than for smaller nozzles. Thus, our initial situation is exactly contrary to the conditions mentioned by Tomiyama et al..[21] Nevertheless, the bifurcation was observed. In addition, our bifurcation appears for droplets formed at the very same nozzle while with the other no bifurcation appears. One explanation could be that if the initial deformation is small, the droplet shape is near to the stable shape that will be established according to the acting forces during drop rise. A higher initial deformation has to be dampened in some way which possibly abet unstable fluid dynamic conditions.

Position of Fig. 4

This is an preprint of an article published in AIChE Journal 56(1) 2-10 (2010), DOI: http://dx.doi.org/10.1002/aic.11969.

What can be stated with certainty is that droplets >3 mm rise in a straight line without velocity oscillation or bifurcation, characteristic mean and maximum velocity are close to each other, see Fig. 4 (at least until the oscillations due to shape deformation occur, beginning at d_P = 4.4 mm). For 2.2 mm ≤ d_P < 3.0 mm, oscillation effects occur which are not related to shape deformation or nozzle type. Maybe, these velocity oscillations can be associated with resonance frequency effects, namely with the eigenfrequency of the droplets. But this is speculative, and further investigations have to be made on this issue.

Fig. 4 shows that for 3.0 mm < d_P < 4.4 mm, characteristic mean and maximum values are close to each other. The droplets are oblate, but non-oscillating. The maximum terminal velocity is achieved by 3.2 mm droplets with v_t = 187 mm/s. For bigger droplets, the terminal velocity slowly decreases. Shape deformation becomes significant for droplets exceeding 4.4 mm. The Weber number for d_P = 4.4 mm is 3.8 and close to the critical values 4.08 and 4.04 proposed by Winnikow & Chao[23] and Krishna et al.[24] respectively. Consequently, characteristic mean and maximum velocities deviate from each other (see as an example Figs. 3e & f). This droplet diameter is in very good agreement with the critical diameter proposed by Klee & Treybal:[13]

$$d_{cr} = 0.33\rho_c^{-0.14}\Delta\rho^{-0.43}\mu_c^{0.3}\sigma^{0.24} \tag{2}$$

Note that in Eq. (2) the following units apply: [ρ] = g/cm³, [μ]=Poise, [σ] = dyn/cm and [d_{cr}] = cm. For toluene droplets in water Eq. (2) yields d_{cr} = 4.45 mm.

Correlation of terminal velocity

In order to calculate the terminal velocity for a clean system, Grace et al.[11] propose to use the general correlation for contaminated systems multiplied with a correction factor which has to be determined experimentally. The resulting formulation is

$$v_{t,pure} = v_t\left(1+\frac{\Gamma}{1+\mu^*}\right) \tag{3}$$

introducing the correction function Γ which is shown in Fig. 5 for toluene drops in water. Grace et al. propose to draw Γ as a function of $\Lambda = Eo(1+0.15\mu^*)/(1+\mu^*)$, this was also adopted in Fig. 5. The higher Γ is, the higher is the terminal velocity compared to the contaminated system. For small and high values of Λ, Γ decreases to 0, in other words, contaminants of the drop surface do not significantly affect the terminal drop rise velocity. We choose the logarithmic density function

$$f(\Lambda) = \alpha \cdot e^{-\frac{(\log\Lambda - \chi)^2}{2\delta^2}} \tag{4}$$

to envelop the experimental data with the parameter $\alpha = 1.7$, $\chi = -0.7$ and $\delta = 0.35$. Together with Eq. (3) and the Eqs. (A.1) - (A.4), see Appendix, $f(\Lambda)$ has been used to draw the dotted line $v_t\left(d_P, f\left[\Lambda\right]\right)$ in Fig. 4. The agreement is very good with the experimental data up to the critical diameter d_{cr} = 4.45 mm. For larger droplets, the curve lies between maximum and characteristic mean velocities and finally slightly underestimates the terminal velocity for the larger droplets investigated here (6 - 7 mm).

Position of Fig. 5

Drag coefficient

Fig. 6 shows a plot of the drag coefficient as a function of Reynolds number. The experimental data are compared with correlations taken from literature, see Appendix Eqs. (A-6) - (A-10), under consideration that the viscosity ratio μ^* for the system toluene/water is ≈ 0.62. All maximum values and the characteristic mean values up to d_P = 2.2 mm are given in the figure. The correlations are represented by continuous lines within the range of validation for the Reynolds number and by dotted lines if this range is exceeded. In addition, the two limiting curves for rigid spheres[25]

$$C_D = \frac{24}{Re} + \frac{3.73}{Re^{0.5}} - \frac{4.83\cdot10^{-3}\,Re^{0.5}}{1+3\cdot10^{-6}\,Re^{1.5}} + 0.49 \qquad (Re < 3\cdot10^5) \tag{5}$$

and for spherical bubbles[26]

$$C_D = \frac{16}{Re} + \frac{14.9}{Re^{0.78}}\left(\frac{1}{1+10Re^{-0.6}}\right) \qquad (Re > 2) \tag{6}$$

are shown for comparison. Furthermore, a line representing the critical Weber number We = 4 (see section 3.1), i.e. $C_D = Mo\,Re^4/48$,[27] is drawn in the figure as well. The results show that the experimental data (both characteristic mean and maximum values) for toluene droplets are situated between the two limiting curves for rigid spheres and spherical bubbles. The smaller the drops are, the closer the drag coefficient is to the rigid sphere curve, but even for the smallest droplets investigated here the drag coefficient is below the rigid sphere curve. This indicates clearly that even droplets in the range of 1 mm do have a moving interface and thus an inner circulation provided that the system is clean enough which seems to be the case here. Drag coefficients in impure system will be considerably higher and will match the rigid sphere curve.

For bigger droplets, the drag coefficient decreases until the minimum drag point is reached ($C_D \approx 0.15$ at $Re \approx 615$ corresponding to d_P = 3 mm). Note that exactly for this diameter the bifurcation has been observed. From this point on, an increase in drop size does not lead to an increase in drop rise velocity but to a slight decrease. This is due to shape deformation which becomes more and more important. Consequently, the drag coefficient increases sharply, approximately around the curve for We = 4.

Position of Fig. 6

A comparison between drag correlations from literature and experimental data is only reasonable for Reynolds numbers below the minimum drag point since the correlations are only valid for fluid spheres. If this range is considered and keeping in mind that drop deformation, strictly speaking, begins already at Re ≈ 200 in the experiments, the following conclusions can be drawn from Fig. 6:

The correlation by Rivkind & Ryskin[28] is only suitable for the toluene/water system when applied strictly in the validation range of Reynolds number (up to Re = 100). Therefore, the agreement is reasonable well for small diameters. When the drag coefficients based on the characteristic mean velocities are compared, the mean deviation is about 8.5%, for the drag coefficients calculated from maximum velocities, the deviation is even better (around 5.5%). For higher Reynolds numbers, the trend of the experimental values cannot be represented by this correlation. The correlation by Hamielec et al.[29] matches the maximum values within 3% in the validation range of Reynolds number (Re < 100), the discrepancy to

the characteristic mean values is about 13.4%. But if the correlation is applied to higher Reynolds numbers, it shows fairly good agreement with the characteristic mean values (between Re = 100 and 300 the deviation is only 3.4%). Even the trend of the maximum values is well represented. The mean deviation is around 4.7% when Reynolds numbers up to the minimum drag point are considered. The only correlation which is valid for Reynolds numbers up to 1000 is the one by Feng & Michaelides.[30] Compared to our experimental results, the correlation slightly underestimates the drag coefficients for all Reynolds numbers considered here. The slope of the maximum values is well reproduced, the mean deviation is 9.1% and 20.3% for maximum and characteristic mean values, respectively, applied again to all Reynolds numbers up to the minimum drag point.

Estimation on wall effects

All experimental studies on droplet motion have to be carried out in containers of finite dimensions, thus wall effects do always affect the fluid dynamic behaviour.[14,31] The presence of confining walls increases the drag and influences the shape of deformable droplets.[31] With existing correlations from literature, the influence of the container walls on drag or terminal drop rise velocity, respectively, can be estimated. In these correlations, the (equivalent) diameter of the container D or the diameter ratio $\lambda = d_P/D$, respectively, appears as a new variable.[32] More details on this issue can be found in the review article by Michaelides.[33]

For viscous spherical droplets in creeping flow, the drag force is given by the Hadamard solution:[34]

$$C_D = K \frac{8}{Re}\left(\frac{2+3\mu^*}{1+\mu^*}\right) \tag{7}$$

with the correction factor K considering the influence of the container wall on the drag as proposed by Haberman & Sayre,[35] see Eq. (A-11) in the Appendix. For droplets of intermediate size (Eo < 40), the wall effects are insignificant (effect on terminal velocity is below 2%) if the following conditions apply:[14]

$$Re \le 0.1 \qquad \lambda \le 0.06 \tag{8}$$

$$0.1 < Re < 100 \qquad \lambda \le 0.08 + 0.02 \log_{10} Re \tag{9}$$

$$Re \ge 100 \qquad \lambda \le 0.12 \tag{10}$$

For Reynolds number exceeding 200, the relation between the terminal drop rise velocity in restricted extent, v_t, and the drop rise velocity in an infinite container, $v_{t,\infty}$, can be expressed with the following equation (up to $\lambda = 0.6$):[14,31]

$$\frac{v_t}{v_{t,\infty}} = \left(1-\lambda^2\right)^{3/2} \tag{11}$$

For the parameter range used in the present work (1.0 mm ≤ d_P ≤ 7.0 mm) λ ranges between 0.0133 and 0.0933. In all cases, λ is smaller than the corresponding critical λ-values in Eqs. (8) - (10), i.e. the wall effect on the terminal drop rise velocity is below 2%. For the 1 mm toluene droplet (λ_{1mm} = 0.0133), the Reynolds number is about 40. If one calculates the correction factor K, although not in creeping flow conditions, one gets K_{1mm} = 1.023, i.e. the drag is only slightly increased (≈ 2.3%). The Reynolds number of 2 mm droplets (λ_{2mm} = 0.0266) is around 250, with Eq. (11) the velocity in infinite media would be only 0.11% higher than in a restricted domain. For the biggest droplet investigated here (d_P ≤ 7.0 mm, λ_{7mm} = 0.0933), the increase is only 1.3%. Hence, the wall effect on the terminal drop rise velocity is - for all droplets investigated in the present study - in the range of the experimental error and therefore not further considered.

Weber-Reynolds diagram

On the basis of a variety of bubble rising experiments in various viscous liquids, Maxworthy et al.[15] propose a correlation for the Weber number which contains - in contrast to the Eötvös number Eo - the terminal drop rise velocity v_t:

$$We = f(Mo)Re^{5/3} \tag{12}$$

with

$$f(Mo) = 0.526\,Mo^{0.358} \tag{13}$$

Fig. 7 shows the *We* vs. *Re* diagram for the results of the present study. Up to $We \approx 0.7$ ($Re \approx 250$), the agreement is excellent. For Weber numbers between 1 and 3.2, the maximum deviation does not exceed 30%. The correlation is not useful anymore for higher Weber numbers since deviations can be up to 150%. As proposed by Maxworthy et al.,[15] Eq. (12) should be used for Reynolds numbers below the minimum drag point and is useful for a first approximation where extreme precision is not necessary.

Position of Fig. 7

Summary and conclusion

Transient rise velocities were systematically measured for toluene droplets in water. The droplet diameter was varied between 1.0 and 7.0 mm. Three nozzles with different diameters were used in order to cover the whole droplet diameter range.

The main objective of this work was to find a correlation describing terminal rise velocities in pure systems. This was done based on a semi-empirical approach by Grace et al.,[11] Eq. (A.5). The necessary correction function Γ was experimentally determined and is given in Fig. 5 whereby the terminal velocity of toluene drops in water can be calculated satisfactorily (Fig. 4). To our knowledge, higher velocities of toluene droplets rising in water have not been reported in literature so far.

Comparisons with drag coefficient correlations found in literature were satisfactory, especially with the one of Hamielec et al.[29] if the range of validation is extended to higher Reynolds numbers. Up to the minimum drag point, the Weber-Reynolds-correlation proposed by Maxworthy et al.[15] is quite suitable for a rough approximation with errors of no more than 30%. The wall effect on drag and terminal drop rise velocity was found to be negligible.

In the course of the experiments, some more interesting results could be observed which were found important to be mentioned:

- In the diameter range 2.4 - 3.0 mm, unexpected oscillations in the drop rise velocity occurred, irrespective of the nozzle type (N_1 or N_2). Thus, deviations between characteristic mean and maximum velocities were found. The reason is unclear yet, maybe eigenfrequency effects could play a role.

- At d_P = 3 mm, the terminal drop rise velocity suddenly increases when nozzle N_1 is used, the oscillation in velocity disappears. For nozzle N_2, two distinct terminal velocities were found. Out of 60 measurements with d_P = 3 mm, about the one half shows oscillations and lower velocity while the other half does not. Comparable bifurcation effects were found by Thorsen et al.[19] for different organic liquids. The reason remains unclear.

- The above mentioned bifurcation appears at the minimum drag point. From that point on, characteristic mean and maximum velocities become close to each other again.

- Significant shape oscillations begin at d_P = 4.4 mm. This value is in very good agreement with the critical diameter proposed by Klee & Treybal,[13] which is d_{cr} = 4.45 mm. Characteristic mean and maximum velocities deviate again from each other.

Droplet movement in cleaner systems tend to be more sophisticated since fluid dynamic instabilities can presumably appear easier than in contaminated systems. In the present work, major effort has been made to keep the system as clean as possible. The benefit was that the different physical phenomena mentioned in this work can be clearly distinguished in the figures and associated with a specified diameter range.

This is an preprint of an article published in AIChE Journal 56(1) 2-10 (2010), DOI: http://dx.doi.org/10.1002/aic.11969.

Appendix

Terminal velocity correlation by Grace et al.[11]

For unpurified systems the terminal velocity can be calculated by:

$$v_t = \frac{\mu_c}{\rho_c d_P} Mo^{-0.149} \left(J - 0.857\right) \tag{A.1}$$

with

$$J = 0.94H^{0.757} \qquad \left(2 < H \le 59.3\right) \tag{A.2}$$

$$J = 3.42H^{0.441} \qquad \left(H > 59.3\right) \tag{A.3}$$

$$H = \frac{4}{3} EoMo^{-0.149} \left(\frac{\mu_c}{\mu_w}\right)^{-0.14} \qquad \text{with } \mu_w = 0.0009 Pas \tag{A.4}$$

For purified systems, the correlation is modified with a semi-empirical approach introducing a correction function Γ:

$$v_{t,pure} = v_t \left(1 + \frac{\Gamma}{1+\mu^*}\right) \tag{A.5}$$

Drag coefficient correlations

Three correlations to calculate the drag coefficient for viscous particles in a continuous phase have been chosen here from literature to be compared with experimental results of this study:

(a) Hamielec et al.[29]

$$C_D = \frac{3.05\left(7.83\mu^{*2} + 2142\mu^* + 1080\right)}{\left(60 + 29\mu^*\right)\left(4 + 3\mu^*\right) Re^{0.74}} \qquad (4 < Re < 100) \tag{A.6}$$

(b) Rivkind & Ryskin[28]

$$C_D = \frac{1}{1+\mu^*}\left[\mu^*\left(\frac{24}{Re} + \frac{4}{Re^{1/3}}\right) + \frac{14.9}{Re^{0.78}}\right] \qquad (10 \le Re \le 100) \tag{A.7}$$

(c) Feng & Michaelides[30]

$$C_D\left(Re, \mu^*\right) = \frac{2-\mu^*}{2} C_D\left(Re, 0\right) + \frac{4\mu^*}{6+\mu^*} C_D\left(Re, 2\right) \qquad (0 \le \mu^* \le 2 \text{ and } 5 \le Re \le 1000) \tag{A.8}$$

with the functions

$$C_D\left(Re,0\right)=\frac{48}{Re}\left(1+\frac{2.21}{\sqrt{Re}}-\frac{2.14}{Re}\right) \tag{A.9}$$

$$C_D\left(Re,2\right)=17.0Re^{-2/3} \tag{A.10}$$

Correction factor K to account for the influence of containing walls on drag coefficient (Haberman & Sayre[35]*)*

$$K=\frac{1+p_1\lambda^5\left(\frac{1\text{-}\mu^*}{2+3\mu^*}\right)}{1-p_2\lambda\left(\frac{2+3\mu^*}{1+\mu^*}\right)+p_3\lambda^3\left(\frac{\mu^*}{1+\mu^*}\right)+p_4\lambda^5\left(\frac{2\text{-}3\mu^*}{1+\mu^*}\right)-p_5\lambda^6\left(\frac{1\text{-}\mu^*}{1+\mu^*}\right)} \tag{A.11}$$

for viscous spherical droplets at creeping flow conditions with the parameters $p_1=2.2757$, $p_2=0.7017$, $p_3=2.0865$, $p_4=0.5689$, $p_5=0.72603$. The correlation shows good agreement for $\lambda \le 0.5$.[14,31]

This is an preprint of an article published in AIChE Journal 56(1) 2-10 (2010), DOI: http://dx.doi.org/10.1002/aic.11969.

Notation

A	surface area (m²)
C_D	drag coefficient (m)
d	diameter (m)
D	column diameter (m)
g	gravity (m/s²)
h_{tr}	travel distance (m)
ID	inner diameter (m)
K	correction factor wall drag (-)
OD	outer diameter (m)
$p_1, p_2 \ldots$	parameters (-)
P	power (W)
t	time (s)
T	temperature (°C)
v_t	terminal drop rise velocity (m/s)

Greek symbols

α	a factor (-)
Γ	correction function (-)
δ	standard deviation (-)
λ	diameter ratio d_P/D (-)
μ	dynamic viscosity (Pa·s)
μ^*	ratio of dynamic viscosities μ_d/μ_c (-)
ρ	density (kg/m^3)
σ	interfacial tension (N/m)
χ	expected value (-)

Dimensionless numbers

Eo	Eötvös number	$\frac{g d_P^2 \Delta\rho}{\sigma}$

Mo	Morton number	$\frac{g\mu_c^4\Delta\rho}{\rho_c^2\sigma^3}$
Re	Reynolds number	$\frac{v_t d_P \rho_c}{\mu_c}$
We	Weber number	$\frac{v_t^2 d_P \rho_c}{\sigma}$
Λ	*Eo*-μ^*-group	$Eo\left(1+0.15\mu^*\right)\Big/\left(1+\mu^*\right)$

Subscripts

c	continuous phase
cha	characteristic
cr	critical
d	dispersed phase
max	maximum
min	minimum
P	particle, drop
t	terminal
tr	travel
w	water
∞	in infinite container

Literature Cited

1. Abdel-Alim AH, Hamielec AE. Theoretical and Experimental Investigation of Effect of Internal Circulation on Drag of Spherical Droplets Falling at Terminal Velocity in Liquid-Media. *Ind Eng Chem Fund.* 1975;14(4):308-312.
2. Garner FH, Skelland AHP. Some factors affecting droplet behaviour in liquid-liquid systems. *Chem Eng Sci.* 1955;4(4):149-158.
3. Calderbank PH, Korchinski IJO. Circulation in liquid drops: (A heat-transfer study). *Chem Eng Sci.* 1956;6(2):65-78.
4. Horton TJ, Fritsch TR, Kintner RC. Experimental Determination of Circulation Velocities Inside Drops. *Canadian J Chem Eng.* 1965;43(3):143-146.
5. Griffith RM. The effect of surfactants on the terminal velocity of drops and bubbles. *Chem Eng Sci.* 1962;17(12):1057-1070.
6. Edge RM, Grant CD. The motion of drops in water contaminated with a surface-active agent. *Chem Eng Sci.* 1972;27(9):1709-1721.
7. Levan D, Newman J. The Effect of Surfactant on the Terminal and Interfacial Velocities of a Bubble or Drop. *AIChE J.* 1976;22(4):695-701.
8. Li X, Mao Z-S, Fei W. Effects of surface-active agents on mass transfer of a solute into single buoyancy driven drops in solvent extraction systems. *Chem Eng Sci.* 2003;58(16):3793-3806.
9. Linde H, Sehrt B. Der Einfluss der Marangoni-Instabilität auf den hydrodynamischen Widerstand der Tropfen im System Benzaldehyd-Essigsäure-Wasser. *Zeitschrift für physikalische Chemie München.* 1966;231(3-4):151-172.
10. Loth E. Quasi-Steady Shape and Drag of Deformable Bubbles and Drops. *Int J Multiphase Flow*. 2008;34(6):523-546.
11. Grace JR, Wairegi T, Nguyen TH. Shapes and velocities of single drops and bubbles moving freely through immiscible liquids. *Trans Instn Chem Engrs.* 1976;54:167-173.
12. Hu S, Kintner RC. The fall of single liquid drops through water. *AIChE J.* 1955;1(1):42-48.
13. Klee AJ, Treybal RE. Rate of rise or fall of liquid drops. *AIChE J.* 1956;2(4):444-447.
14. Clift R, Grace JR, Weber ME. Bubbles, Drops and Particles. New York: Academic Press, 1978.

15. Maxworthy T, Gnann C, Kürten M, Durst F. Experiments on the rise of air bubbles in clean viscous liquids. *J Fluid Mech.* 1996;321:421-441.

16. Wegener M, Fevre M, Wang Z, Paschedag AR, Kraume M. Marangoni convection in single drop flow - Experimental investigations and 3D-simulations. International Conference on Multiphase Flow: Leipzig, Germany; 2007.

17. Misek T, Berger R, Schröter J. Standard test systems for liquid extraction. *Inst Chem Eng., EFCE Publication Series.* 1985;46

18. Wegener M, Grünig J, Stüber J, Paschedag AR, Kraume M. Transient rise velocity and mass transfer of a single drop with interfacial instabilities - experimental investigations. *Chem Eng Sci.* 2007;62(11):2967-2978.

19. Thorsen G, Stordalen RM, Terjesen SG. On the terminal velocity of circulating and oscillating liquid drops. *Chem Eng Sci.* 1968;23(5):413-426.

20. Wu M, Gharib M. Experimental studies on the shape and path of small air bubbles rising in clean water. *Phys Fluids.* 2002;14(7):49-52.

21. Tomiyama A, Celata GP, Hosokawa S, Yoshida S. Terminal velocity of single bubbles in surface tension force dominant regime. *Int J Multiphase Flow.* 2002;28(9):1497-1519.

22. Yang B, Prosperetti A, Takagi S. The transient rise of a bubble subject to shape or volume changes. *Phys Fluids.* 2003;15(9):2640-2648.

23. Winnikow S, Chao BT. Droplet Motion in Purified Systems. *Phys Fluids.* 1966;9(1):50-61.

24. Krishna PM, Venkateswarlu D, Narasimhamurty GSR. Fall of Liquid Drops in Water. Terminal Velocities. *J Chem Eng Data.* 1959;4(4):336-340.

25. Brauer H. Momentum, Mass, and Heat-Transfer through Boundary Surface of Spherical-Particles. *Chem Ing Tech.* 1973;45(18):1099-1103.

26. Brauer H. Particle/Fluid Transport Processes. *Fortschritte der Verfahrenstechnik* 1979;17:61-99.

27. Harper JF. The motion of bubbles and drops through liquids. *Adv Appl Mech.* 1972;12:59-129.

28. Rivkind VY, Ryskin GM. Flow structure in motion of a spherical drop in a fluid medium at intermediate Reynolds numbers. *J Fluid Dynamics* 1976;11(1):5-12.

29. Hamielec AE, Storey SH, Whitehead JM. Viscous flow around fluid spheres at intermediate Reynolds-numbers. *Canadian J Chem Eng.* 1963;12:246-251.

30. Feng Z-G, Michaelides EE. Drag Coefficients of Viscous Spheres at Intermediate and High Reynolds Numbers. *J Fluids Eng.* 2001;123:841-849.

31. Michaelides EE. Particles, Bubbles & Drops, World Scientific Publishing Singapur, 2006.

32. Harmathy TZ. Velocity of large drops and bubbles in media of infinite or restricted extent. *AIChE J.* 1960;6(2):281-288.

33. Michaelides EE. Hydrodynamic Force and Heat/Mass Transfer From Particles, Bubbles, and Drops - The Freeman Scholar Lecture. *J Fluids Eng.* 2003;125(2):209-238.

34. Hadamard JS. Mouvement permanent lent d'une sphère liquide et visqueuse dans un liquide visqueux. *C R Acad Sci Paris.* 1911;152:1735-1743.

35. Haberman WL, Sayre RM. Motion of rigid and fluid spheres in stationary and moving liquids inside cylindrical tubes. *Rep. No. 1143, David Taylor Model Basin.* 1958

This is an preprint of an article published in AIChE Journal 56(1) 2-10 (2010), DOI: http://dx.doi.org/10.1002/aic.11969.

Figure captions

Fig. 1: Experimental setup. (1) glass column, (2) jacket, (3) thermostat, (4) precision dosing pump (Hamilton PSD/2), (5) nozzle for drop formation, (6) solenoid device, (7) saturation tank, (8) high speed camera, (9) illumination, (10) computer control.

Fig. 2: Scheme for determination of maximum and characteristic mean velocity (v_{max} and v_{cha} respectively) of a recorded sequence. In this figure, two sequences for different diameters are presented. The maximum and characteristic mean velocity has to be averaged over all recorded sequences of one droplet diameter.

Fig. 3: Transient drop rise velocity of toluene drops rising in water. 3a) One representative recorded sequence for 1.0, 1.4, 1.8 and 2.2 mm (nozzle N_1). 3b) Oscillation effects for 2.4, 2.6 and 2.8 mm (nozzle N_2). 3c) 15 sequences of 3 mm droplets when nozzle N_1 is used. 3d) Bifurcation for 3 mm droplets when nozzle N_2 is used. 7 sequences show oscillating behaviour, 8 do not. 3e) Three sequences for 4.8 mm droplets (nozzle N_3). 3f) One typical sequence for 5.6 mm (nozzle N_3).

Fig. 4: Terminal velocity as a function of droplet diameter for toluene drops rising in water. Comparison of maximum and characteristic mean values of the terminal velocity for the three nozzles used in the experiments. The correlation by Grace et al.[11] is given for comparison.

Fig. 5: Factor Γ giving the correction in terminal velocity in pure systems. Experimental data and logarithmic distribution density function plotted versus Λ.

Fig. 6: Drag coefficient as a function of Reynolds number. Comparison of experimental results and correlations from literature.

Fig. 7: Weber number as a function of Reynolds number. Comparison of experimental results with correlation by Maxworthy et al..[15]

This is an preprint of an article published in AIChE Journal 56(1) 2-10 (2010), DOI: http://dx.doi.org/10.1002/aic.11969.

Table 1: Nozzle characteristics.

	N_1	N_2	N_3
OD [mm]	<0.5	1	3
ID [mm]	<0.1	0.5	2
$d_{P,min}$ [mm]	1.0	2.0	4.8
$d_{P,max}$ [mm]	3.6	5.0	7.0
material	borosilicate	borosilicate	stainless steel

Table 2: Physical parameters for toluene and water at $T = 25°C$.[17]

	ρ [kg/m³]	μ [10^{-4}·Pa s]	σ [mN/m]	μ^*	Mo
toluene	862.3	5.52	35	0.62	$1.95 \cdot 10^{-11}$
water	997.02	8.903			

This is an preprint of an article published in AIChE Journal 56(1) 2-10 (2010), DOI: http://dx.doi.org/10.1002/aic.11969.

Fig. 1

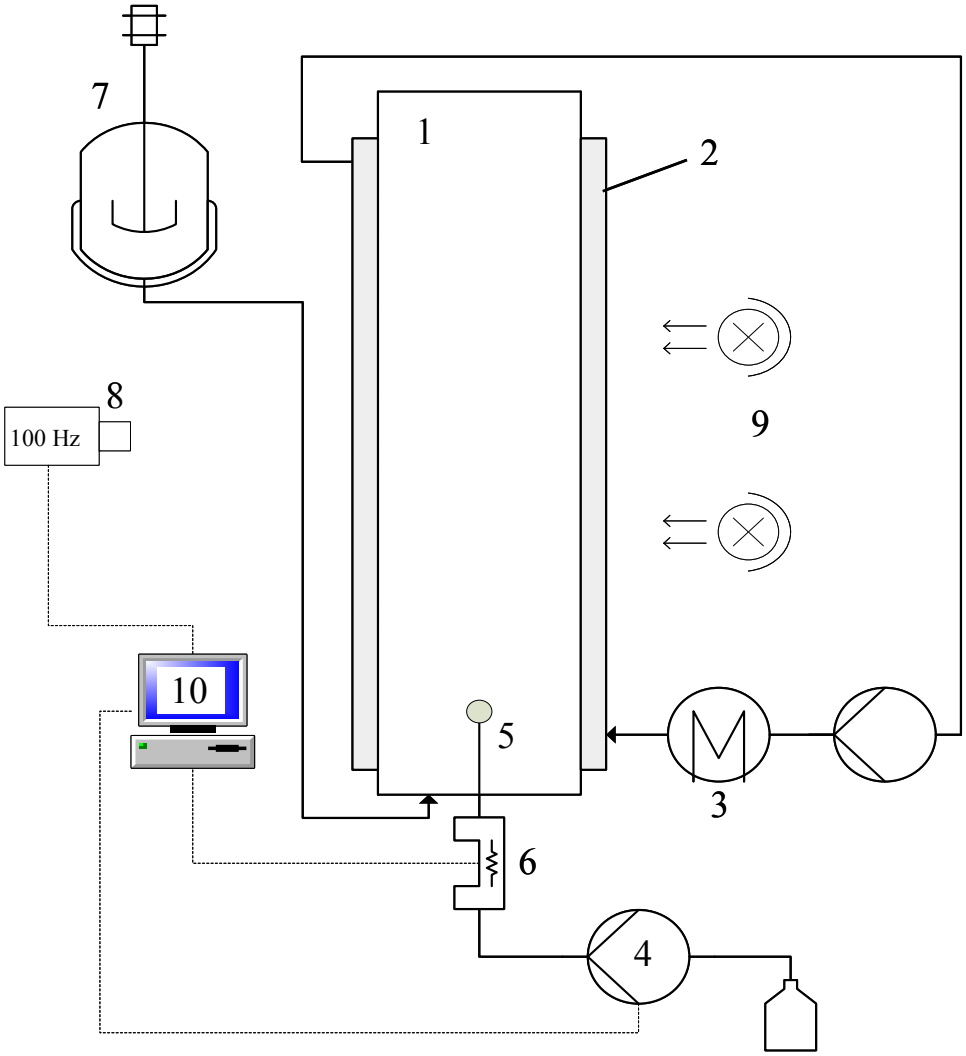

This is an preprint of an article published in AIChE Journal 56(1) 2-10 (2010), DOI: http://dx.doi.org/10.1002/aic.11969.

Fig. 2

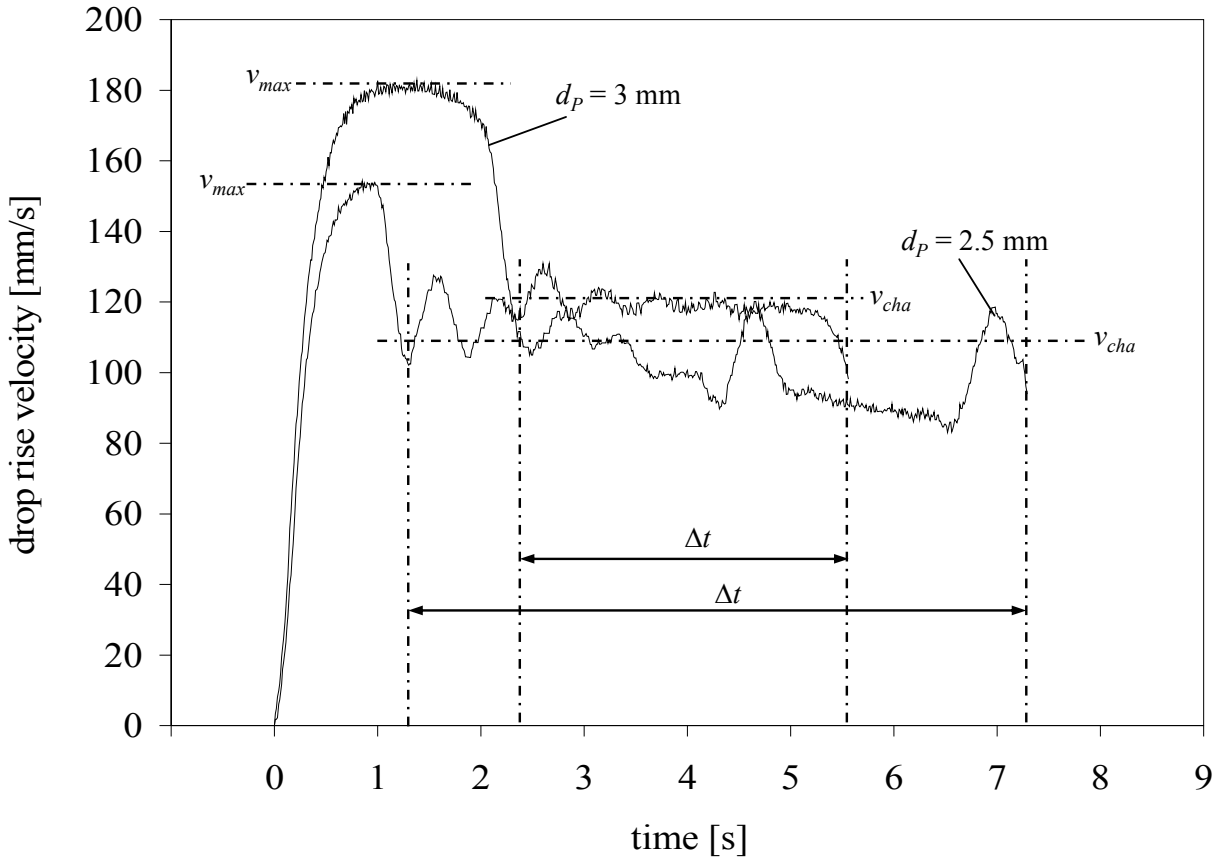

This is an preprint of an article published in AIChE Journal 56(1) 2-10 (2010), DOI: http://dx.doi.org/10.1002/aic.11969.

Fig. 3

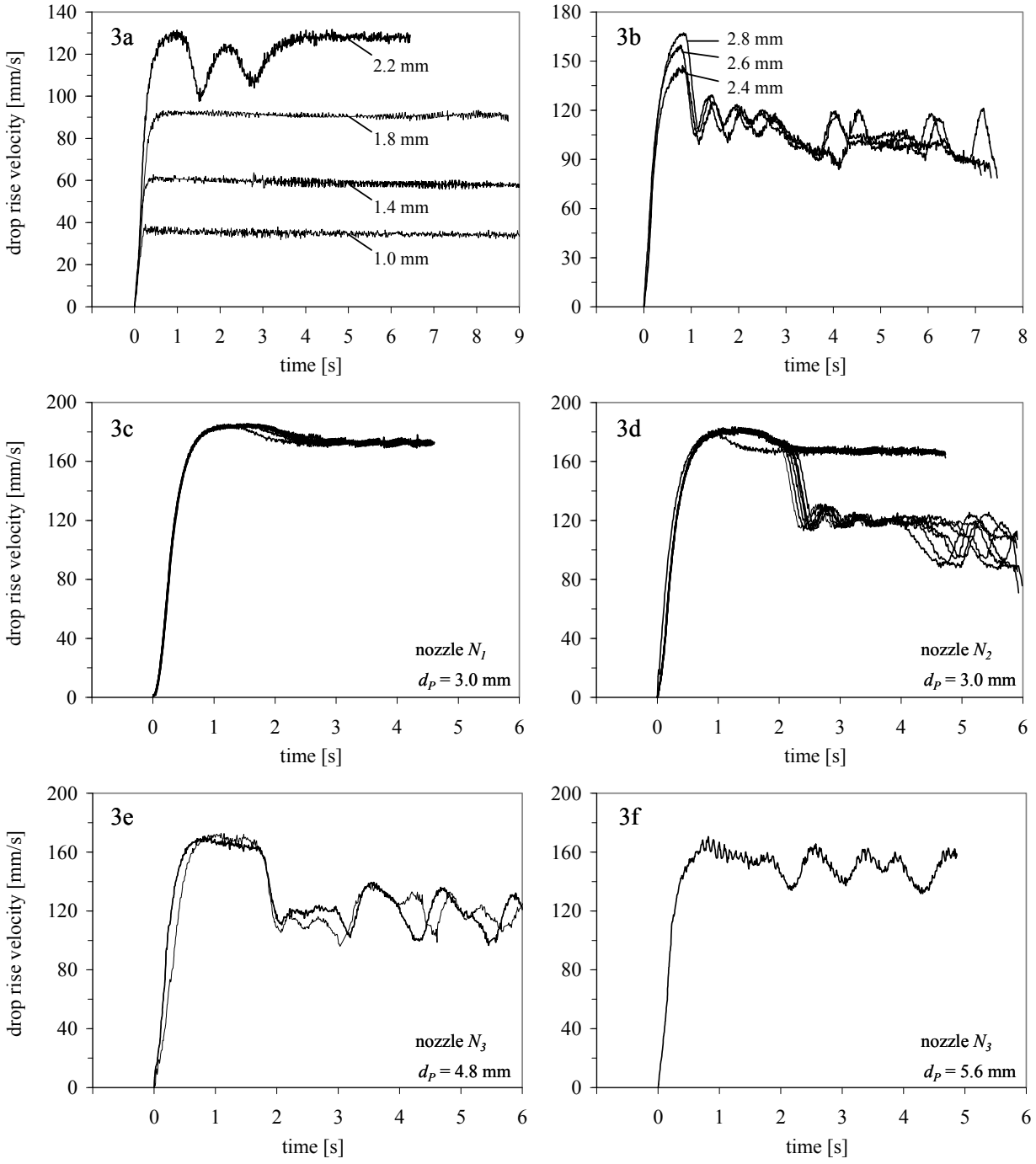

This is an preprint of an article published in AIChE Journal 56(1) 2-10 (2010), DOI: http://dx.doi.org/10.1002/aic.11969.

Fig. 4:

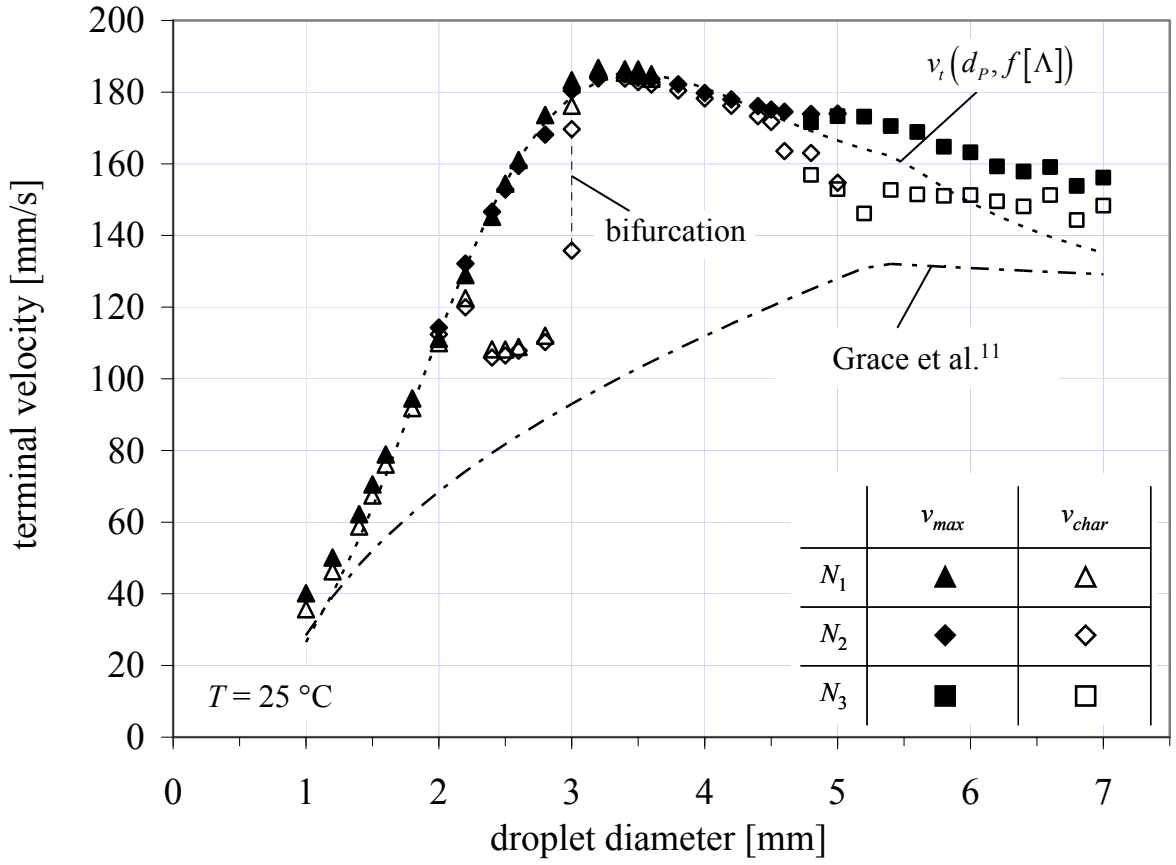

This is an preprint of an article published in AIChE Journal 56(1) 2-10 (2010), DOI: http://dx.doi.org/10.1002/aic.11969.

Fig. 5:

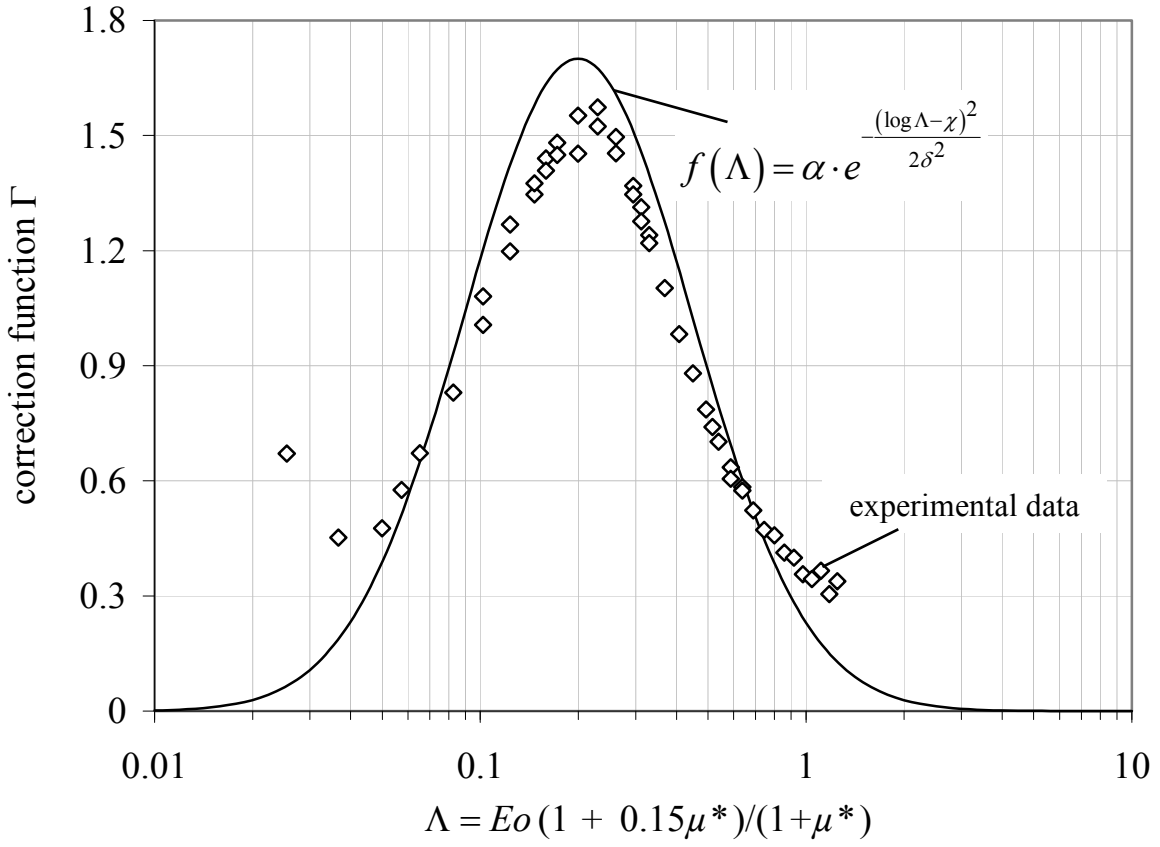

This is an preprint of an article published in AIChE Journal 56(1) 2-10 (2010), DOI: http://dx.doi.org/10.1002/aic.11969.

Fig. 6:

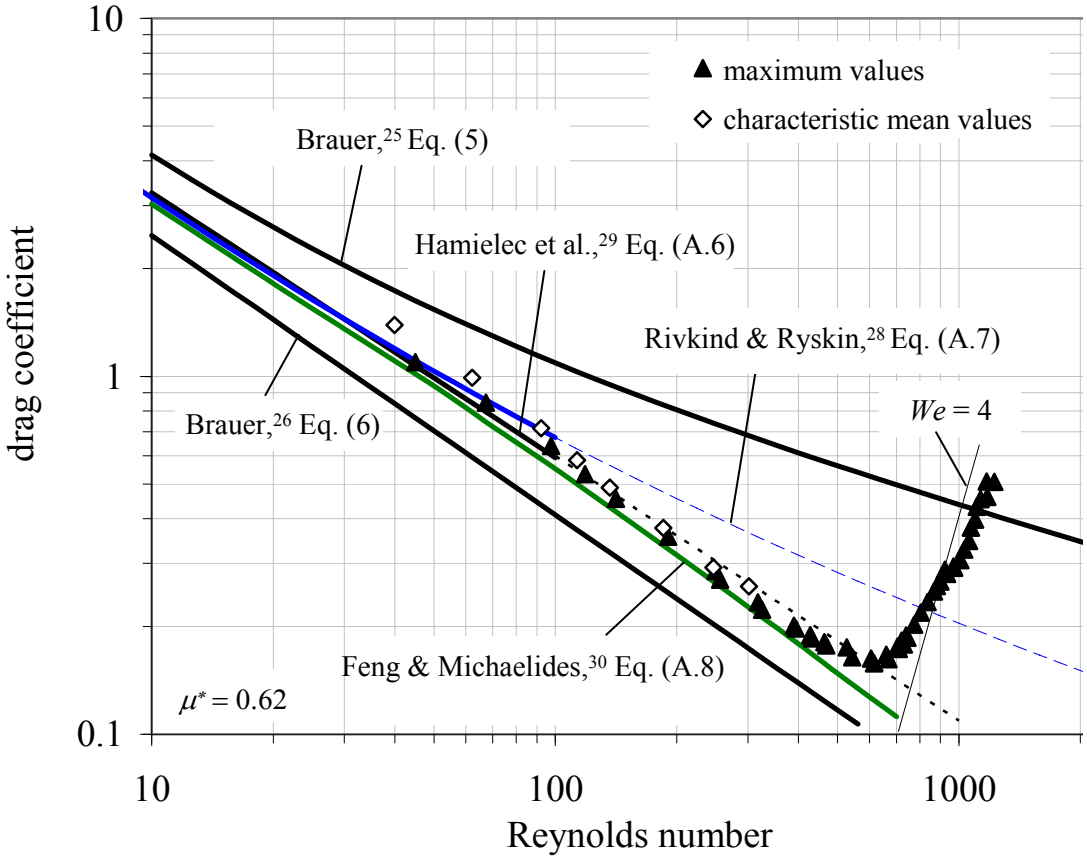

This is an preprint of an article published in AIChE Journal 56(1) 2-10 (2010), DOI: http://dx.doi.org/10.1002/aic.11969.

Fig. 7: